Available online at www.sciencedirect.com
SCIENCE DIRECT®
Journal of Sound and Vibration 261 (2003) 309–328
JOURNAL OF SOUND AND VIBRATION
www.elsevier.com/locate/jsvi

# Optimal design of engine mount using an artificial life algorithm

Young Kong Ahn, Jin Dae Song, Bo-Suk Yang*

*School of Mechanical Engineering, Pukyong National University, San 100, Yongdang-dong, Nam-gu, Pusan 608-739, South Korea*

Received 22 October 2001; accepted 23 May 2002

**Abstract**

When designing fluid mounts, design parameters can be varied in order to obtain a desired notch frequency and notch depth. The notch frequency is a function of the mount parameters and is typically selected by the designer to occur at the vibration disturbance frequency. Since the process of choosing these parameters can involve some trial and error, it seems to be a great application for obtaining optimal performance of the mount. Many combinations of parameters are possible to give us the desired notch frequency, but the question is which combination provides the lowest depth? Therefore, an automatic optimal technique is needed to optimize the fluid mount.

In this study, the enhanced artificial life algorithm (EALA) is applied to minimizing transmissibility of a fluid mount at the desired notch frequency, and at the notch and resonant frequencies. The present hybrid algorithm is the synthesis of a conventional artificial life algorithm with the random tabu search (R-tabu) method and then, the time for searching optimal solution could be reduced from the conventional artificial life algorithm and its solution accuracy became better.

The results show that the performance of the optimized mount by using the hybrid algorithm has been better than that of the conventional fluid mount.


## 1. Introduction

Mounts are commonly used to connect two structures together to prevent vibration transmission from one to the other. Passive mounts consist of a resilient element that is designed to statically hold the structures together and dynamically isolate them from each other. A major challenge in designing mounts, particularly elastomeric mounts, is to make them statically stiff

*Corresponding author. Tel.: +82-51-620-1604; fax: +82-51-620-1405.
*E-mail addresses:* ahn@mail1.pknu.ac.kr (Y.K. Ahn), bsyang@pknu.ac.kr (B.-S. Yang).

0022-460X/03/$ - see front matter © 2002 Elsevier Science Ltd. All rights reserved.
PII: S0022-460X(02)00989-6

and dynamically soft. Elastomeric mounts are rubber-to-metal bonded elements that are widely used for a variety of industrial applications.

The dynamic stiffness of an elastomeric mount increases with increasing disturbance frequency. Therefore, stiffening the mount to achieve a better connection results in poorer isolation at high frequency. On the other hand, reducing the dynamic stiffness requires a lower static stiffness and weaker ability to hold the structures together. In a manner analogous to a spring, dynamic stiffness for an elastomeric mount is defined as the ratio between the forces applied to the mount and the displacement that it causes across the mount.

To overcome some of the drawbacks of elastomeric mounts, fluid mounts are often used to provide a better compromise between the static and dynamic requirements of the mount [1–3]. Following studies performed, modelling of a fluid mount [4–10], its optimization [11–16], and development of various engine mounts [17] have been presented by many researchers.

The resonance caused by fluid passing between the two compliant rubber chambers can either provide additional damping to the fundamental mount resonance, or create a tuned absorber effect to provide a superior isolation at a single frequency depending on how the mount is designed.

The tuned absorber effect of the fluid results in a dynamic stiffness "notch" at which the transmissibility and the dynamic stiffness are low and the isolation effectiveness is high. Therefore, fluid mounts can be designed to have a much higher static stiffness (e.g., as much as 1.5–2 times) than elastomeric mounts, with substantially higher isolation capability (by as much as 10 times, or 20 dB) at the disturbance frequency. Because of their added isolation benefits, fluid mounts are used in many cars, trucks, and buses. More recently, they have been selected for aerospace applications such as aircraft engine mounts and helicopter pylon isolators [4]. When designing fluid mounts, there are many designing parameters that the engineers can vary in order to obtain the desired notch frequency and notch depth. Since the process of choosing these parameters can involve some trial and error, it seems to be a great application for the optimization of the mounts. There are many combinations of parameters possible to obtain the desired notch frequency, but the question is which combination provides the lowest notch depth.

In general, it is not easy to optimize such a non-linear optimization problem by some conventional optimization methods that have the probability of being converged into a local optimum solution. On the other hand, an artificial life algorithm has recently received attention regarding its capability as a global optimization technique for complex, linear, non-linear, and multi-optimization problems, and has been successfully applied to several engineering problems [18–20].

In this paper, the performance of the fluid mount is first investigated by varying the designing parameters. Then, the enhanced artificial life algorithm (EALA) [21] was employed to minimize the transmissibility of a fluid mount at the desired notch frequency. The advantage of the artificial life algorithm is that any kind of objective functions can converge to stable global solution and does not need to calculate derivatives of the function for the optimization. Even though the fundamental resonant mode has much more vibration energy than the notch frequency mode, we are interested in the design parameters chosen to obtain the optimal performance of the fluid mount at the desired notch frequency because the notch frequency is the main vibration disturbance frequency. However, minimizing the transmissibility at the fundamental and notch frequencies was additionally investigated.

Results show that the transmissibility of the optimized mount at the notch frequency lowered more than that of the original mount. Furthermore, the optimization results by the EALA were compared with those of the sequential quadratic programming (SQP) [22].

## 2. Fluid mount

Fig. 1 shows the configuration of a fluid mount. This device has performance characteristics compatible with the mounts commonly used for applications such as isolating large turbofan engines from the air frame in commercial aircraft [23]. The inner member is connected to the sources of vibration (e.g., engine), and the outer member is connected to the structure to be isolated (e.g., air frame). The fluid mount is an elastomeric mount with fluid travelling between two rubber-enclosed chambers. A fluid passage between the two chambers, called an ''inertia track'', is used to connect them. The inertia track can be external in the main embodiment of the mount, as shown in Fig. 1, or internal in the mount. Furthermore, a small volume compensator is often used to accommodate the change in fluid volume due to the temperature change. The compensator consists of a fluid cavity that is connected to one of the fluid chambers through a small valve, and a small nitrogen-charged chamber that is separated from the fluid by a bladder [24]. The small valve between the compensator and the fluid chamber allows fluid passage statically to accommodate fluid volume changes, but blocks fluid passage at higher frequencies to dynamically decouple the compensator from the fluid chamber.

## 3. Fluid mount model

Fig. 2 shows the fluid/mechanical model for the fluid mount shown in Fig. 1. A dynamic pressure is created on the piston area $A_p$ (the piston area of the upper and lower chambers) due to the force $F$ applied to the inner member that is connected to the vibration source. The force $F$ causes the displacement $x$ between the inner and outer members. The flow rates $Q_1$, $Q_2$, and $Q_3$ are used in the development of the corresponding linear differential equations. $Q_1$ and $Q_3$ are equal and correspond to the flow in and out of the upper and lower fluid chambers shown in

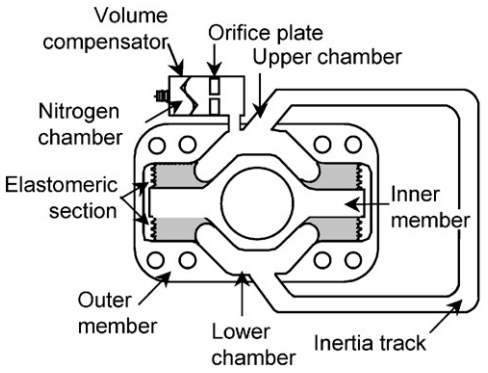


Fig. 1. Schematic representation of the fluid mount with external inertia track.

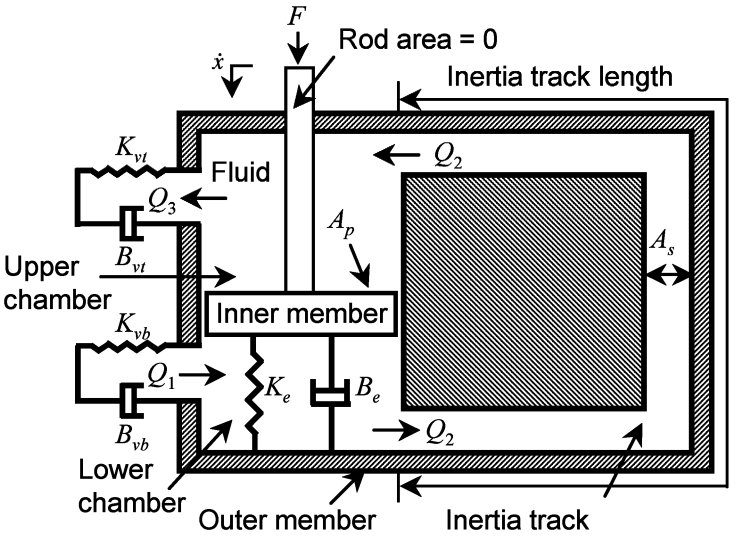


Fig. 2. Fluid/mechanical model of the fluid mount.

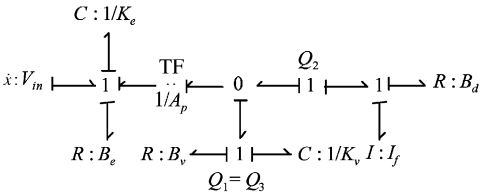


Fig. 3. Bond graph model of the fluid mount.

Fig. 2. The volumetric stiffness of the upper and lower chambers, $K_{vt}$ and $K_{vb}$ and the volumetric damping coefficients of the upper and lower chambers, $B_{vt}$ and $B_{vb}$, can be combined as follows:

$$K_v = K_{vt} + K_{vb}, \quad B_v = B_{vt} + B_{vb}. \tag{1}$$

It is worth noting that the above equations do not include tensile forces since rubber elements are not able to withstand repeated tensile force without incurring damage. When the inner member is displaced relative to the outer member, a restoring force is created due to the elastomer, which is modeled by the parallel spring $K_e$ and damper $B_e$.

The fluid mount model of Fig. 2 has two different energy domains of hydraulic domain and of mechanical domain for elastomer. The bond graph model is well known as a convenient means of representing multiple energy-domain systems [15,25], which is employed to develop a linear model of the fluid mount in this study. Moreover, the bond graph model has another advantage of reducing the parameter numbers. The bond graph model has been used in the modelling of hydraulic mount by many researchers, the standard techniques exits for modelling fluid and mechanical capacitances, viscous damping, capillary flow, and relations between fluid pressures and mechanical forces. A bond graph representing the fluid/mechanical model of the mount is

shown in Fig. 3. Using the bond graph model, we can write the equations for the flow rates as

$$Q_2 = Q_3 + A_p\dot{x}, \tag{2}$$

$$Q_1 = Q_3. \tag{3}$$

Further, the bond graph implies

$$\dot{p}_I = -\frac{(B_v + B_d)}{I_f}p_I - K_v q_v + A_p B_v \dot{x}, \tag{4}$$

$$\dot{q}_v = -\frac{1}{I_f}p_I - A_p\dot{x}, \tag{5}$$

$$\dot{q}_e = \dot{x}, \tag{6}$$

where $p_I$ is the momentum of fluid inertia $I_f$, $q_v$ is the volumetric displacement of combined volumetric stiffness $K_v$, $B_d$ is fluid resistance in the inertia track, and $q_e$ is the displacement of the spring representing the elastomer stiffness $K_e$. Additionally, the equation for the force $F$ can be derived from the bond graph as

$$F = K_e q_e + (B_e + A_p^2 B_v)\dot{x} - A_p K_v q_v - \frac{A_p B_v}{I_f}p_I. \tag{7}$$

Assuming sinusoidal motion, Eqs. (4)–(6) can be expressed as follows:

$$\begin{bmatrix} \mathrm{j}\omega + (B_v + B_d)/I_f & K_v \\ -1/I_f & \mathrm{j}\omega \end{bmatrix} \begin{Bmatrix} P_I \\ q_v \end{Bmatrix} = \begin{Bmatrix} B_v A_p \\ -A_p \end{Bmatrix} \mathrm{j}\omega x, \tag{8}$$

$$q_e = x. \tag{9}$$

Substitution of $P_I$ and $q_v$ obtained by using Cramer's rule in Eq. (8), and Eq. (9) into the force $F$ given by Eq. (7) yields

$$F = K_e x + \mathrm{j}\omega x(B_e + A_p^2 B_v) - A_p K_v \frac{\{A_p I_f \omega^2 - \mathrm{j}\omega A_p(B_d + B_v) + A_p B_v \mathrm{j}\omega\}x}{K_v + \mathrm{j}\omega(B_d + B_v) - I_f\omega^2} - A_p B_v \frac{\{A_p K_v \mathrm{j}\omega - \mathrm{j}\omega A_p B_v \omega^2\}x}{K_v + \mathrm{j}\omega(B_d + B_v) - I_f\omega^2}. \tag{10}$$

The ratio between the force $F$ and the displacement $x$ is called the dynamic stiffness $K^*$ of the mount, and is given by

$$K^* = \frac{F(s)}{x(s)} = K_e + s(B_e + A_p^2 B_v) + \frac{A_p^2\{sK_v(B_d - B_v) - B_v^2 s^2 + K_v I_f s^2\}}{K_v + s(B_d + B_v) + I_f s^2}, \tag{11}$$

where $s$ is the Laplace operator. Rewriting Eq. (11) in the frequency domain through using $s = \mathrm{j}\omega$, where $\mathrm{j} = \sqrt{-1}$ and $\omega$ is the dynamic frequency in rad/s, yields

$$K^* = K' + \mathrm{j}K'', \tag{12}$$

where

$$K' = K_e + A_p^2 \times \frac{\omega^2\{I_f\omega^2(K_vI_f - B_v^2) - K_v(K_vI_f - B_d^2)\}}{(K_v - I_f\omega^2)^2 + \omega^2(B_d + B_v)^2}, \tag{13}$$

$$K'' = (B_e + A_p^2B_v)\omega + A_p^2 \times \frac{K_v^2(B_d - B_v)\omega + \omega^3\{2K_vB_vI_f - B_v^2(B_d + B_v)\}}{(K_v - I_f\omega^2)^2 + \omega^2(B_d + B_v)^2}. \tag{14}$$

The real stiffness $K'$ represents the stiffness properties of the mount, while $K''$ indicates its damping properties. Assuming there is no damping (i.e., $B_e = B_v = B_d = 0$), the dynamic stiffness in Eq. (11) exhibits an undamped pair of poles and an undamped pair of zeros. The maximum value for the dynamic stiffness occurs at the poles

$$\omega_{rs} = \sqrt{K_v/I_f}, \tag{15}$$

the resonant frequency of the mount by fluid passing. The minimum value for the dynamic stiffness occurs at the zeros

$$\omega_{ns} = \sqrt{\frac{K_eK_v}{(K_e + A_p^2K_v)I_f}} \quad \text{or} \quad \omega_{ns} = \omega_{rs}\sqrt{\frac{K_e}{K_e + A_p^2K_v}}, \tag{16}$$

the notch frequency of the mount. As indicated by Eqs. (15) and (16), the fluid resonant frequency $\omega_{rs}$ (rad/s) due to fluid passing is always greater than the notch frequency $\omega_{ns}$. Furthermore, the dynamic stiffness is equal to $K_e$ at low frequencies and $K_e + K_vA_p^2$ at high frequencies, as evident from Eq. (11) with assuming no damping. The dynamic stiffness is used to demonstrate the isolation effectiveness of the mount. Lowering the dynamic stiffness results in a higher dynamic isolation of the mount at the notch frequency.

Another useful measure in assessing the isolation effectiveness of the mount is the dynamic transmissibility $T$, which is defined as the ratio between the output and input forces. Using the real stiffness $K'$, imaginary stiffness $K''$ and the mass $M_1$ supported by the mount, we can obtain the transmissibility as follows:

$$T = \left[\frac{K'^2 + K''^2}{(K' - M_1\omega^2)^2 + K''^2}\right]^{1/2} = (T_n/T_d)^{1/2}, \tag{17}$$

where

$$\begin{aligned} T_n = {} & \omega^2\{B_vK_e + B_eK_v + B_d(K_e + A_p^2K_v) - (B_e + A_p^2B_v)I_f\omega^2\}^2 \\ & + [K_eK_v - \{B_vB_e + B_d(B_e + A_p^2B_v) + I_f(K_e + A_p^2K_v)\}\omega^2]^2, \end{aligned}$$

$$\begin{aligned} T_d = {} & \omega^2[B_vK_e + B_eK_v + B_d(K_e + A_p^2K_v) - \{(B_e + A_p^2B_v)I_f + (B_d + B_v)M_1\}\omega^2]^2 \\ & + [K_eK_v - \{B_vB_e + B_d(B_e + A_p^2B_v) + I_f(K_e + A_p^2K_v) + K_vM_1\}\omega^2 + I_fM_1\omega^4]^2. \end{aligned}$$

Assuming no damping (i.e., $B_e = B_v = B_d = 0$), the transmissibility in Eq. (17) exhibits an undamped pair of poles and an undamped pair of zeros. The maximum value for the transmissibility occurs at the poles

$$\omega_{r1} = \sqrt{\frac{A - \sqrt{(-4I_f K_e K_v M_1 + A^2)}}{2I_f M_1}}, \tag{18}$$

$$\omega_{r2} = \sqrt{\frac{A + \sqrt{(-4I_f K_e K_v M_1 + A^2)}}{2I_f M_1}}, \tag{19}$$

where

$$A = I_f K_e + A p^2 I_f K_v + K_v M_1.$$

The resonant frequency $\omega_{r1}$ is the fundamental resonant frequency of the mount. The fluid resonant frequency $\omega_{r2}$ due to fluid passing between the two compliant rubber chambers and is almost equal to the frequency $\omega_{rs}$ of Eq. (15). The minimum value for the transmissibility occurs at the zeroes, which means that the transmissibility has the notch at the zeros. The notch frequency of the transmissibility is exactly the same that of the dynamic stiffness.

## 4. Parametric study of fluid mount

A parametric study using the transmissibility Eq. (17) was conducted to see how sensitive location of the notch and fluid resonant frequencies and the notch depth were to the design parameters. This study is important to determine which parameters need the most accurate estimation. The following parameters were considered for the study:

- Rubber stiffness
- Volumetric damping
- Piston area
- Fluid inertia: $I_f = \rho L/A_s$
- Volumetric stiffness

Original parameters of the fluid mount listed in Table 1 taken from Refs. [4,5] except the sprung mass were varied by $\pm 30\%$. The cases with negative error indicate parameter underestimation and the cases with positive error represent parameter overestimation. The parameters of the fluid resistance and the elastomeric damping were not considered because their variation is too small to alter the mount performance in the study. As shown in Fig. 4(a), changing the rubber stiffness $K_e$ greatly affects the fundamental resonant frequency, the notch frequency and the transmissibility at the notch frequency. As expected, lowering the rubber stiffness results in a lower fundamental resonant frequency of the mount, a lower notch frequency and a lower transmissibility at the

Table 1
Mount parameters used in numerical simulation

| Parameters | Value |
|---|---|
| Piston area $A_p$ | $0.00839\,m^2$ |
| Inertia track area $A_s$ | $7.1 \times 10^{-5}\,m^2$ |
| Fluid elastomeric $B_d$ | $6.4 \times 10^6\,N.s/m^5$ |
| Elastomeric damping $B_e$ | $17.5\,N\,s/m$ |
| Volumetric damping $K_e$ | $5.78 \times 10^7\,N/m$ |
| Elastometric stiffness $K_v$ | $4.15 \times 10^{11}\,N/m^5$ |
| Inertia track length $L$ | $0.17\,m$ |
| Fluid density $\rho$ | $1.765 \times 10^3\,kg/m^3$ |
| Sprung mass $M_1$ | $3.7 \times 10^5\,kg$ |

notch and fundamental resonant frequencies. This parameter is one of the easiest parameters to measure in a fluid mount.

The performance of the mount according to the parameter variations except rubber stiffness was only observed around the notch and fluid resonant frequencies because the volumetric damping and stiffness, the piston area and the fluid inertia are closely related with both the frequencies. The notch, fluid resonant and fundamental resonant frequencies can be calculated from Eqs. (16), (19) and (18), respectively.

Fig. 4(b) shows that the volumetric or bulge damping $B_v$ greatly affects the mount transmissibility at the notch frequency. The notch depth of underestimating volumetric damping is lower than that of overestimating volumetric damping. Since underestimating volumetric damping reduces damping ratios of the modes of the notch and fluid resonant frequencies, the transmissibility at the notch frequency decreases but the transmissibility at the fluid resonant frequency increases. Although not easy to analytically predict as some of the parameters, the volumetric damping can be measured in a given mount.

Fig. 4(c) shows that the piston area $A_p$, which is defined as the effective area of the fluid cavity that pumps the fluid into the inertia track, greatly affects the mount transmissibility at the notch frequency. Overestimating the piston area lowers the notch frequency and the transmissibility at the notch frequency, but raises the transmissibility at the fluid resonant frequency. However, the fluid resonant frequency does not change. The piston area can be estimated accurately either through direct measurement or through geometric analysis of the fluid cavity.

The volumetric or bulge stiffness $K_v$ of the mount has a similar effect on the mount transmissibility as the piston area because the amount of the volumetric stiffness is proportionate to the piston area. As shown in Fig. 4(d), the overestimation of the volumetric stiffness lowers the transmissibility at the notch frequency and also increases the notch and fluid resonant frequencies. However, The variation of the volumetric stiffness has an almost no effect on the transmissibility at the fluid resonant frequencies. Estimating analytically the volumetric stiffness is not easy and therefore, the parameter has to be measured in a given mount.

The properties of the fluid inertia $I_f$ affect little the transmissibility at the notch and fluid resonant frequencies, but has a great effect on both the frequencies. As shown in Fig. 4(e), the underestimation of the fluid inertia increases both the frequencies. The fluid inertia can be estimated accurately either through direct measurement or through analytical prediction.

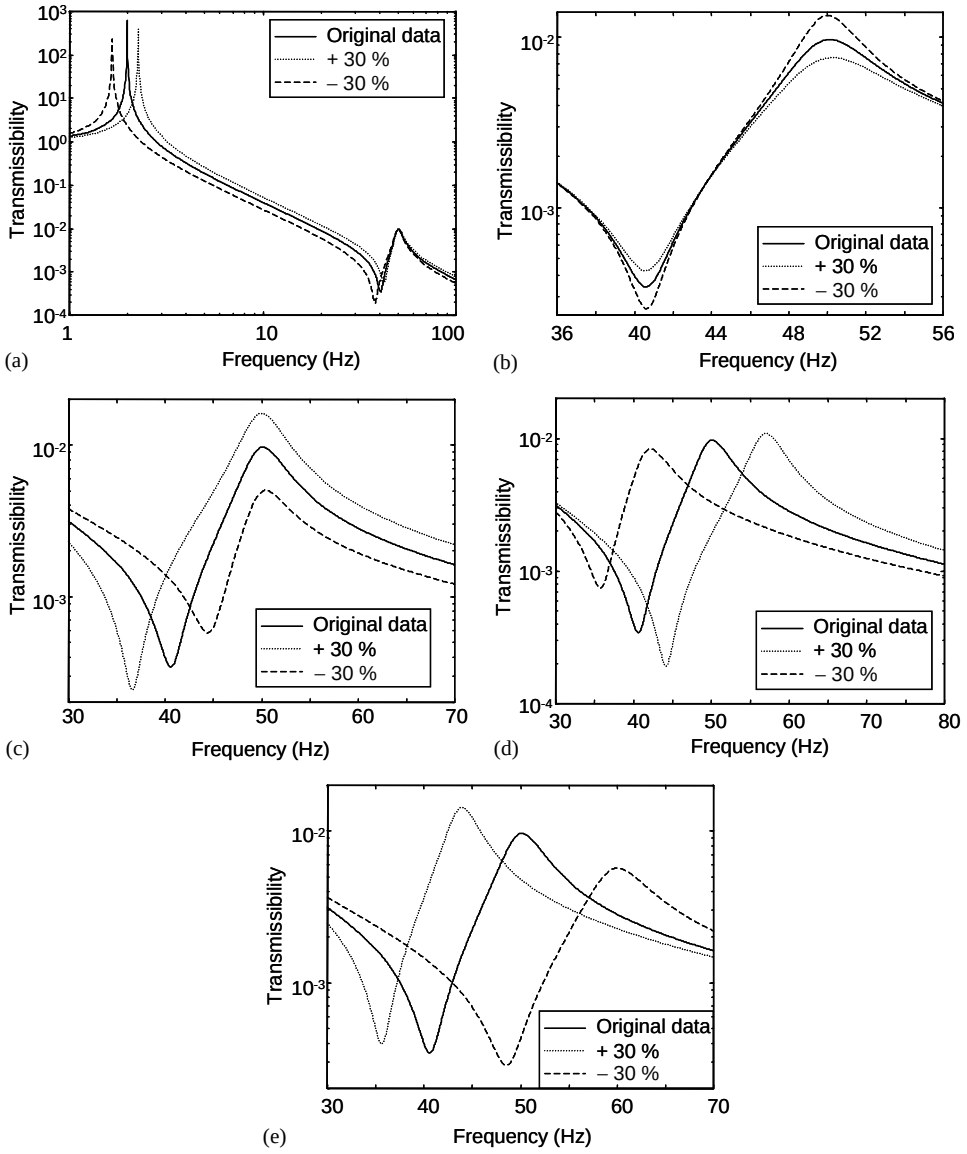


Fig. 4. Effect of design parameters on transmissibility. (a) Rubber stiffness $K_e$; (b) volumetric damping $B_v$; (c) piston area $A_p$; (d) volumetric stiffness $K_v$; (e) fluid inertia $I_f$.

## 5. Optimal design of fluid mount

The EALA [21] is applied for choosing optimum parameters for obtaining optimal performance of the fluid mount. Artificial world in the EALA is defined as the domain of the given optimization problem. The artificial organisms colonize emergently around the optimal solutions by metabolism, movement and reproduction of the organisms, and the optimal solution is given by the location of an artificial organism having the best fitness.

The solution accuracy and calculating speed of the artificial life algorithm are greatly affected by the method of deciding the locations of the resource, the offspring and movement of the organisms. Therefore, the R-tabu method [26] was employed to determine the locations for being in the region nearest to the optimum point. The colonization at the EALA with R-tabu method can be formed more quickly and compactly than the conventional artificial life algorithm [21]. It means that the calculating speed to find the optimum solution and solution accuracy in the artificial life algorithm depends on the speed and density of forming colonization. Therefore, the hybrid algorithm is improved in the calculating speed and the accuracy of solution [21]. The calculation procedure of the EALA shown in Fig. 5 is as follows.

*Step 1*. Initialization: There are four kinds of species and resources, respectively. Individual numbers of the species and resources have the same number as the other. All the organisms with the internal energy $I_e$ and the resources are randomly distributed in the artificial world.

*Step 2*. Search: The artificial organisms look for the nearest resource needed for metabolism within their neighborhood region. Here the neighborhood region is defined as follows:

$$C = \{x \in R^n \mid \|x - x_s\| \leqslant D\}, D = D_0 e^{-(t/T)\gamma},$$

$x_s$: the current location of an arbitrary organism
$D_0 = 1$: the initial value

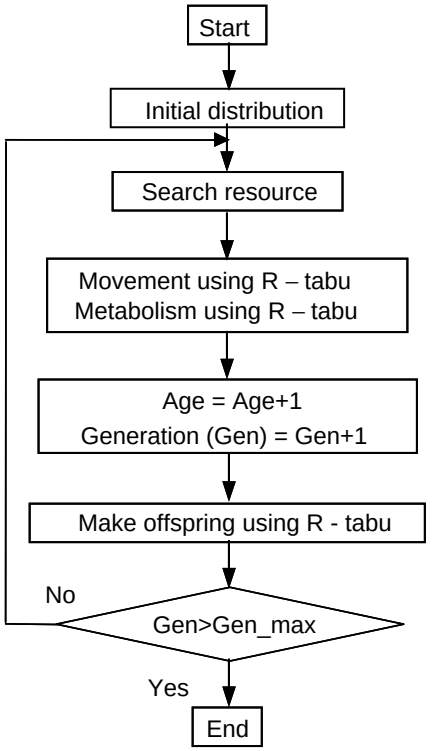


Fig. 5. Flow chart of the optimization algorithm.

$t$: the current generation number
$T = 3000$: the last generation number
$\gamma = 12$: the constant
$n = 6$: the number of design variables

*Step 3*. Metabolism: First, if the organisms find the resources in the region, they move to the nearest location of the resources. Then they get the metabolism energy $G_e$ through the metabolism with resources and also randomly produce wastes in the neighborhood region. The locations of the wastes are decided by the R-tabu method as with the following description. First of all, the neighborhood region is divided into as many sub-regions as step size $N_s$. In the next place, a location is randomly selected for a step. If the function value of the selected location is better than one of the current locations, the selected location is saved as the candidate location of the waste. If not, a location is randomly selected over again until the selection number is the same as that of the count number $N_c$, or satisfaction of this condition. Finally, after the process is conducted for all steps, the best candidate location among the candidate locations is selected as the location of the waste.

*Step 4*. Random movement: If the organisms could not find any resource within their neighborhood region, their locations will be changed randomly by using the R-tabu method. The elite organisms defined as the organisms belonging to the upper 90% in fitness get as much energy as the elite energy $E_e$.

*Step 5*. Increasing age & generation: In this process, the artificial organism's age and generation are increased by 1.

*Step 6*. Reproduction: If the organism's age and its internal energy are more than the adult age $R_a$ and the adult energy $R_e$ respectively, an organism reproduces two offspring with a mate of the same species according to the reproducing probability $R_p$. The location of one offspring is decided by using R-tabu method within the neighborhood region of one parent, and that of the other offspring is done within the neighborhood region of the other parent.

*Step 7*. Reducing energy: To extinguish the organisms with low fitness the internal energy of each organism is decreased by the reducing energy $L_e$. If an artificial organism's energy drops below the defined energy level $L_i$ to survive, it is considered to be dead and is removed from the artificial world.

In returning to Step 2, this process is iterated until the final generation. Some conventional optimal algorithms require derivatives of an objective function, but the EALA does not do any gradient information of the function and also finds global optimal solutions without dependency on the initial value of the design parameters. The parameters of the EALA in this study are listed in Table 2. The design parameters of the fluid mount listed in Table 1 were taken as the design variables as follows:

$$\mathbf{X} = \{A_p \; B_d \; B_v \; B_e \; I_f\}^{\mathrm{T}}, \tag{20}$$

where $I_f = \rho L/A_s$.

The parameters, $B_v$ and $B_e$ are commonly treated as the functions of stiffness as follows:

$$B_e = \alpha K_e, \; B_v = \beta K_v, \; \alpha = 3.03 \times 10^{-7}, \; \beta = 2.53 \times 10^{-4}. \tag{21}$$

Table 2
Parameters used in the EALA

| Parameters | Value | Parameters | Value |
|---|---|---|---|
| $E_e$ | 10 | $R_a$ | 3 |
| $G_e$ | 50 | $R_e$ | 150 |
| $I_e$ | 150 | $R_p$ | 0.0002 |
| $L_e$ | 5 | $N_c$ | 3 |
| $L_i$ | 125 | $N_s$ | 5 |

The present optimization problem with the weight factors $\alpha_1$, $\alpha_2$ and scale factors $\beta_1(= 1/T_{r1}(\mathbf{X}_0)), \beta_2(= 1/T_{ns}(\mathbf{X}_0))$ is formulated as

$$\text{Find } \mathbf{X} \text{ which minimizes } f(\mathbf{X}) = \alpha_1\beta_1 T_{r1}(\mathbf{X}) + \alpha_2\beta_2\ T_{ns}(\mathbf{X})$$
$$\text{subject to the constraints } 0.7\mathbf{X}_0 < \mathbf{X} < 1.3\mathbf{X}_0, \tag{22}$$

where $\mathbf{X}_0$ is the original parameters in Table 1, and $T_{r1}(\mathbf{X})$ and $T_{ns}(\mathbf{X})$ are the dynamic transmissibilities of the mount at the fundamental resonant and desired notch frequencies respectively. A mount requires minimizing the transmissibility at the vibration disturbance frequency and therefore, the notch frequency is selected to occur at the disturbance frequency. The weight factors was defined as $\alpha_1 = 0$ and $\alpha_2 = 1$ to minimize just the transmissibility $T_{ns}(\mathbf{X})$ . To illustrate the solution accuracy of the EALA its optimized results were compared with those of the well-known SQP as a conventional optimization method. The optimized mount parameters by the EALA and SQP are shown in Table 3, and the transmissibilities of the original and optimized mounts are shown in Fig. 6. Fig. 6(b) shows the transmissibilities zoomed around notch frequency. The $\text{SQP}_{\text{min}}$, $\text{SQP}_{\text{mid}}$ and $\text{SQP}_{\text{max}}$ are named according to the initial values of the design parameters defined by the minimum, middle and maximum values respectively.

In Table 3 the optimized parameters by the EALA are exactly the same as those by the $\text{SQP}_{\text{min}}$, but are different from those by the $\text{SQP}_{\text{mid}}$ and $\text{SQP}_{\text{max}}$. The volumetric damping parameters $B_v$ by $+30\%$ calculated from the $\text{SQP}_{\text{min}}$ and EALA are contrary to the result of the parametric study in Fig. 4(b). The reason why the volumetric damping was increased through the optimization is that the notch depth of overestimating the volumetric stiffness treated as the volumetric damping function lowers more than that of underestimating volumetric damping.

To obtain good isolation, we must keep the transmissibility as low as possible. The dash-dot line of the $\text{SQP}_{\text{min}}$ is not visible in Fig. 6 because the line is overlapped under the solid line of the EALA. The optimized mounts for the notch frequency mode, by using the EALA and $\text{SQP}_{\text{min}}$, have a much lower transmissibility than the original mount and the mounts optimized by the $\text{SQP}_{\text{mid}}$ and $\text{SQP}_{\text{max}}$. The optimization results show that the solution accuracy of the SQP depends on the initial design parameters, while the performance of the mount optimized by the EALA has the same that of the best mount among the mounts optimized by the SQP.

The transmissibility of the mount optimized by the EALA for the notch frequency mode compared with that of the original mount decreased by about 75.68% and the fluid resonant frequency by about 30.34%. Even though the design parameters were chosen to obtain the

Table 3
Optimal parameters of the optimized mount for the notch frequency mode

| | Original value | $SQP_{min}$ | | $SQP_{mid}$ | | $SQP_{max}$ | | EALA | |
|---|---|---|---|---|---|---|---|---|---|
| | | Optimal value | Remark (%) | Optimal value | Remark (%) | Optimal value | Remark (%) | Optimal value | Remark (%) |
| $A_p$ ($mm^2$) | 8390.0 | 10907.0 | 30.00 | 10907.0 | 30.00 | 10907.0 | 30.00 | 10907.0 | 30.00 |
| $A_s$ ($mm^2$) | 71.000 | 71.000 | 0.00 | 71.000 | 0.00 | 71.000 | 0.00 | 71.000 | 0.00 |
| $B_d$ ($MN \cdot s/m^5$) | 6.4000 | 4.4800 | −30.00 | 5.3413 | −16.54 | 8.2920 | 29.56 | 4.4800 | −30.00 |
| $B_e$ ($N \cdot s/m$) | 17.500 | 12.250 | −30.00 | 12.250 | −30.00 | 12.250 | −30.00 | 12.250 | −30.00 |
| $B_v$ ($N \cdot s/m^5$) | 105.20 | 136.76 | 30.00 | 119.99 | 14.06 | 136.76 | 30.00 | 136.76 | 30.00 |
| $K_e$ (MN/m) | 57.800 | 40.460 | −30.00 | 40.460 | −30.00 | 40.460 | −30.00 | 40.460 | −30.00 |
| $K_v$ ($GN/m^5$) | 415.00 | 539.50 | 30.00 | 473.35 | 14.06 | 539.50 | 30.00 | 539.50 | 30.00 |
| $L$ (m) | 0.1700 | 0.12900 | −24.12 | 0.12236 | −28.03 | 0.12899 | −24.13 | 0.12900 | −24.12 |

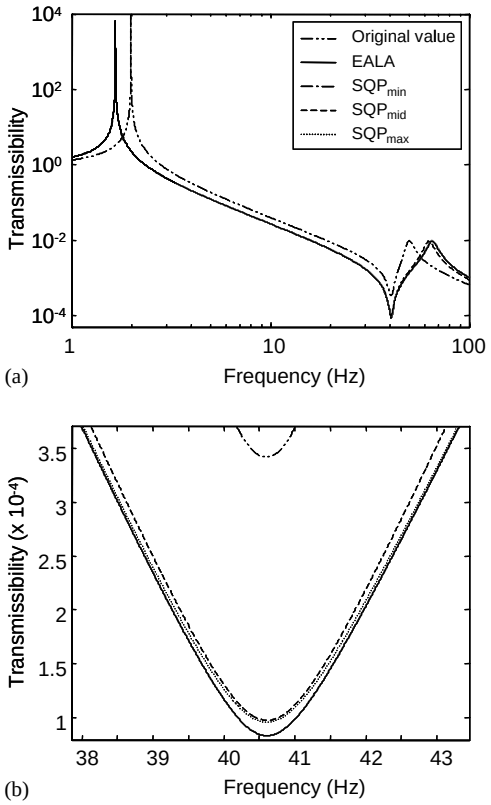


Fig. 6. Transmissibility of the original mount and the optimized mount for the notch frequency mode. (a) Transmissibility for the frequency region from 1 Hz to 100 Hz; (b) transmissibility zoomed around the notch frequency.

optimal performance of the mount at the desired notch frequency, the transmissibility at the fundamental resonant frequency for the optimized mount by the EALA compared with that of the original mount decreased by about 31.23% and the fundamental resonant frequency also decreased by about 16.34%.

Comparison of the dynamic stiffness plots among the original mount and the mounts optimized for the notch frequency mode by the EALA and SQP are shown in Fig. 7, and the dynamic stiffness plots zoomed around the notch frequency are shown in Fig. 7(b). The dash-dot line of the $SQP_{min}$ is not visible in Fig. 7 because the line is overlapped under the solid line of the EALA. The optimized mount by using the EALA and $SQP_{min}$ has a lower dynamic stiffness at the notch frequency compared with that of the original mount and the mounts optimized by the $SQP_{mid}$ and $SQP_{max}$, and provides better isolation using the vibration absorbing effect of the oscillating fluid in the mount. The dynamic stiffness at the notch and fluid resonant frequencies decreased and increased by about 75.67 and 69.15% respectively. The optimization results shown in Figs. 6 and 7 were summarized in Table 4.

Obtaining the optimal performance of the mount for the notch frequency mode is very important. However, the fundamental resonant mode of the mount has a much more vibration

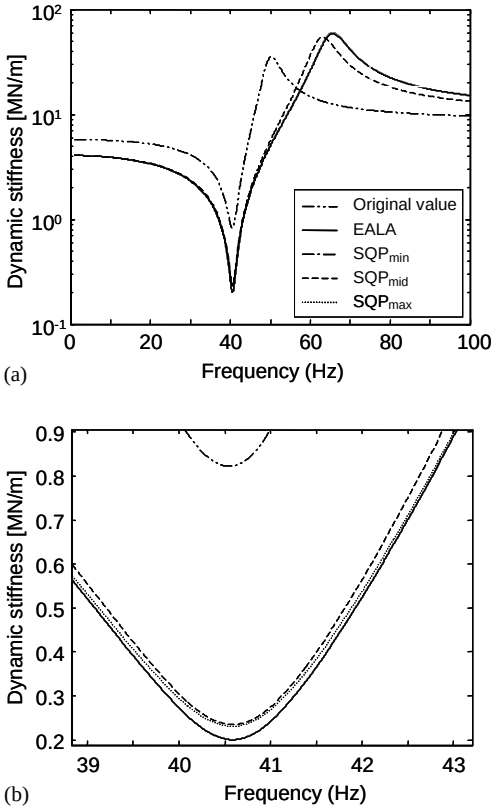


Fig. 7. Dynamic stiffness of the original mount and the optimized mount for the notch frequency mode. (a) Dynamic stiffness for the frequency region from 1 Hz to 100 Hz; (b) dynamic stiffness zoomed around the notch frequency.

energy than the notch frequency mode. Therefore, another study for minimizing the transmissibility at the fundamental and notch frequencies was additionally investigated with weight factor $\alpha_1 = 1$ and $\alpha_2 = 1$ and their results are shown in Fig. 8. Fig. 8(b) shows the transmissibilities zoomed around notch frequency. The optimized parameters by the EALA and SQP are shown in Table 5. The dot line of the $SQP_{max}$ is not visible in Fig. 8 because the line is overlapped under the solid line of the EALA.

The performance and design parameters of the optimized parameters by the EALA shown in Fig. 8 and Table 5 respectively are almost the same that by the $SQP_{max}$ but not by the $SQP_{min}$, and the mounts optimized by the EALA and $SQP_{max}$, have much lower transmissibility than the original mount and the mounts optimized by the $SQP_{min}$ and $SQP_{mid}$. The optimization result of the $SQP_{min}$ is meaningless because the notch frequency obtained by the $SQP_{min}$ differs greatly from the desired notch frequency of 40.6 Hz.

The transmissibility of the mount optimized by the EALA at the fundamental and notch frequencies compared with that of the original mount decreased by about 60.98% and 71.97% respectively, and the fluid resonant frequency increased by about 30.45%. Since the design parameters were chosen to obtain the optimal performance of the mount at the modes of the

Table 4
Property of the original mount and the optimized mount for the notch frequency mode

| | Original value | $SQP_{min}$ | | $SQP_{mid}$ | | $SQP_{max}$ | | EALA | |
|---|---|---|---|---|---|---|---|---|---|
| | | Optimal value | Remark (%) | Optimal value | Remark (%) | Optimal value | Remark (%) | Optimal value | Remark (%) |
| $T_{r1}$ ($\times 10^3$) | 9.6351 | 6.6253 | −31.24 | 5.9425 | −38.32 | 3.7869 | −60.70 | 6.6257 | −31.23 |
| $K^*_{r1}$ (MN · s/m) | 57.753 | 40.418 | −30.02 | 40.420 | −30.01 | 40.418 | −30.02 | 40.418 | −30.02 |
| $\omega_{r1}$ (Hz) | 1.988 | 1.663 | −16.34 | 1.664 | −16.34 | 1.663 | −16.34 | 1.663 | −16.34 |
| $T_{ns}$ ($\times 10^{-5}$) | 34.180 | 8.3136 | −75.68 | 9.7419 | −71.50 | 9.5810 | −71.97 | 8.3147 | −75.68 |
| $K^*_{ns}$ (MN · s/m) | 8.2291 | 2.0021 | −75.67 | 2.3471 | −71.48 | 2.3082 | −71.95 | 2.0020 | −75.67 |
| $\omega_{ns}$ (Hz) | 40.60 | 40.61 | 0.02 | 40.61 | 0.03 | 40.61 | 0.02 | 40.61 | 0.02 |
| $T_{r2}$ ($\times 10^{-3}$) | 9.6737 | 9.6099 | −0.66 | 9.3717 | −3.12 | 9.3579 | −3.27 | 9.6102 | −0.66 |
| $K^*_{r2}$ (MN · s/m) | 354.59 | 599.78 | 69.15 | 541.38 | 52.68 | 584.13 | 64.73 | 599.78 | 69.15 |
| $\omega_{r2}$ (Hz) | 50.15 | 65.36 | 30.35 | 62.89 | 25.41 | 65.37 | 30.36 | 65.36 | 30.34 |

Table 5
Optimal parameters of the optimized mount for the modes of the notch and fluid resonant frequencies

| | Original value | $SQP_{min}$ | | $SQP_{mid}$ | | $SQP_{max}$ | | EALA | |
|---|---|---|---|---|---|---|---|---|---|
| | | Optimal value | Remark (%) | Optimal value | Remark (%) | Optimal value | Remark (%) | Optimal value | Remark (%) |
| $A_p$ ($mm^2$) | 8390.0 | 10 907.0 | 30.00 | 10 907.0 | 30.00 | 10 907.0 | 30.00 | 10 907.0 | 30.00 |
| $A_s$ ($mm^2$) | 71.000 | 71.000 | 0.00 | 71.000 | 0.00 | 71.000 | 0.00 | 71.000 | 0.00 |
| $B_d$ (MN · s/$m^5$) | 6.4000 | 8.3200 | 30.00 | 8.3200 | 30.00 | 8.3200 | 30.00 | 8.3095 | 29.84 |
| $B_e$ (N · s/m) | 17.500 | 14.880 | −14.97 | 17.517 | 0.10 | 12.255 | −29.97 | 12.250 | −30.00 |
| $B_v$ (N · s/$m^5$) | 105.20 | 136.76 | 30.00 | 136.76 | 30.00 | 136.76 | 30.00 | 136.76 | 30.00 |
| $K_e$ (MN/m) | 57.800 | 49.147 | −14.97 | 57.856 | 0.10 | 40.476 | −29.97 | 40.460 | −30.00 |
| $K_v$ (GN/$m^5$) | 415.00 | 539.50 | 30.00 | 539.50 | 30.00 | 539.50 | 30.00 | 539.50 | 30.00 |
| $L$ (m) | 0.1700 | 0.19932 | 17.25 | 0.15806 | −7.02 | 0.12901 | −24.11 | 0.12881 | −24.23 |

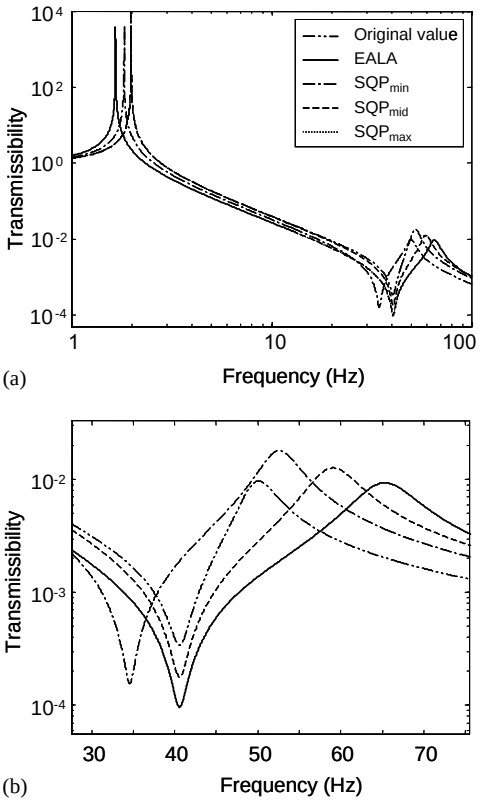


Fig. 8. Transmissibility of the original mount and the optimized mount for the modes of the notch and fluid resonant frequencies. (a) Transmissibility for the frequency region from 1 Hz to 100 Hz; (b) transmissibility zoomed around the notch frequency.

fundamental and notch frequencies, the transmissibility at the fundamental resonant frequency decreased more than that shown in Fig. 6, while the transmissibility at the notch frequency did not do more than that shown in Fig. 6.

Comparison of the dynamic stiffness plots among the original and the mounts optimized by the EALA and SQP for the modes of the notch and fluid resonant frequencies are shown in Fig. 9. The dot line of the $SQP_{max}$ is not visible in Fig. 9 because the line is overlapped under the solid line of the EALA. The optimized mount by using the EALA and $SQP_{max}$ has a lower dynamic stiffness at the notch frequency compared with that of the original mount and the mounts optimized by the $SQP_{min}$ and $SQP_{mid}$. The dynamic stiffness at the notch and fluid resonant frequencies decreased and increased by about 71.92% and 64.60%, respectively. The optimization results shown in Figs. 7 and 8 are summarized in Table 6.

## 6. Conclusions

When designing fluid mounts, many design parameters can be varied in order to obtain the desired notch frequency and depth. It is not easy to obtain the optimal performance of the

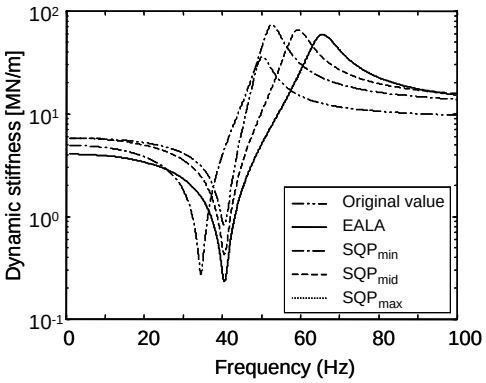


Fig. 9. Dynamic stiffness of the original mount and the optimized mount for the modes of the notch and fluid resonant frequencies.

Table 6
Property of the original mount and the optimized mount for the modes of the notch and fluid resonant frequencies

| | Original value | $SQP_{min}$ | | $SQP_{mid}$ | | $SQP_{max}$ | | EALA | |
|---|---|---|---|---|---|---|---|---|---|
| | | Optimal value | Remark (%) | Optimal value | Remark (%) | Optimal value | Remark (%) | Optimal value | Remark (%) |
| $T_{r1}$ ($\times 10^3$) | 9.6351 | 4.2122 | −56.28 | 4.5499 | −52.78 | 3.8053 | −60.51 | 3.7591 | −60.98 |
| $K^*_{r1}$ (MN·s/m) | 57.753 | 49.068 | −15.04 | 57.783 | 0.05 | 40.434 | −29.99 | 40.419 | −30.02 |
| $\omega_{r1}$ (Hz) | 1.988 | 1.833 | −7.83 | 1.989 | 0.03 | 1.664 | −16.32 | 1.663 | −16.34 |
| $T_{ns}$ ($\times 10^{-5}$) | 34.180 | 1.5638 | −5.4267 | 17.664 | −48.32 | 9.5961 | −71.92 | 9.5805 | −71.97 |
| $K^*_{ns}$ (MN·s/m) | 8.2291 | 2.7347 | −6.6785 | 4.2563 | −48.28 | 2.3119 | −71.91 | 2.3111 | −71.92 |
| $\omega_{ns}$ (Hz) | 40.60 | 34.59 | −14.80 | 40.62 | 0.03 | 40.61 | 0.03 | 40.64 | 0.09 |
| $T_{r2}$ ($\times 10^{-3}$) | 9.6737 | 17.972 | 85.78 | 12.702 | 31.30 | 9.3584 | −3.26 | 9.3380 | −3.47 |
| $K^*_{r2}$ (MN·s/m) | 354.59 | 726.38 | 104.85 | 648.22 | 82.81 | 584.06 | 64.71 | 583.67 | 64.60 |
| $\omega_{r2}$ (Hz) | 50.15 | 52.61 | 4.92 | 59.13 | 17.91 | 65.36 | 30.35 | 65.41 | 30.45 |

mount at the notch frequency in the iteration process of choosing the parameters with trial and error.

In this study, the performance of the fluid mount was investigated according to variation of the designing parameters. Then the EALA was applied to get the optimal performance of the fluid mount at the desired notch frequency, and at the notch and fluid resonant frequencies. To illustrate the solution accuracy of the EALA its optimized results were compared with those of the well-known SQP as a conventional optimization method. The advantage of the artificial life algorithm is that any kind of objective functions can converge to stable global solution and does not need to calculate derivatives of the function for the optimization. However, the SQP requires gradient information of the function.

The results of the parametric study will be helpful to a fluid mount designer. The mount optimized by the EALA has much lower transmissibility than the original mount and its

performance is the same as that of the best mount among the mounts optimized by the SQP. The properties of the EALA are that any gradient information of the objective function is not needed in the algorithm and the global optimal solutions of the function can be always found without dependency on the initial value of the design parameters. However, since the optimization result by the SQP depends on the initial value of the design parameters, its design iteration would need to be repeated with a different set of initial parameters.

## References

[1] H.J. Taylor, The new generation of engine mount, Proceedings of the SAE Milwaukee Section Lecture Series, Milwaukee, WI, SAE Paper 86052, 1986.
[2] Z. Nakajima, C. Matsuoka, S. Okuya, The development of the hydraulic strut mount, Proceedings of the SAE Passenger Car Meeting and Exposition, Detroit, MI, SAE Paper 901729, 1990.
[3] W.C. Flower, Understanding hydraulic mounts for improved vehicle noise vibration and ride qualities, SAE Paper 850975, 1985.
[4] L.R. Miller, M. Ahmadian, C.M. Nobles, D.A. Swanson, Modeling and performance of an experimental active vibration isolator, Transactions of American Society of Mechanical Engineers, Journal of Vibration and Acoustics 117 (3A) (1995) 272–278.
[5] N. Vahdati, A detailed mechanical model of a double pumper fluid mount, Transactions of American Society of Mechanical Engineers, Journal of Vibration and Acoustics 120 (1998) 361–370.
[6] A. Geisberger, A. Khajepour, F. Golnaraghi, Non-linear modeling of hydraulic mounts: theory and experiment, Journal of Sound and Vibration 249 (2) (2002) 371–397.
[7] J.E. Colgate, C.-T. Chang, Y.-C. Chiou, W.K. Liu, L.M. Keer, Modeling of a hydraulic engine mount focusing on response to sinusoidal and composite excitations, Journal of Sound and Vibration 184 (3) (1995) 503–528.
[8] R. Singh, G. Kim, P.V. Ravindra, Linear analysis of automotive hydro-mechanical mount with emphasis on decoupler characteristics, Journal of Sound and Vibration 158 (2) (1992) 219–243.
[9] S.J. Gau, J.D. Cotton, Experimental study and modeling of hydraulic mount and engine system, SAE Paper 951348, 1995.
[10] Z. Nakajima, C. Matsuoka, S. Okuya, The development of hydraulic strut mount, SAE Paper 901729, 1990.
[11] X. Chen, H. Qiand, Y. Zhang, Optimal design of a two-stage mounting isolation system by the maximum entropy approach, Journal of Sound and Vibration 243 (4) (2001) 591–599.
[12] K. Seto, K. Sawatari, A. Nagamatsu, M. Ishihama,K. Doi, Optimum design method for hydraulic mount, SAE Paper 911055, 1991.
[13] J.S. Tao, G.R. Liu, K.Y. Lam, Design optimization of marine engine-mount system, Journal of Sound and Vibration 235 (3) (2000) 477–494.
[14] S. Bouchillon, R. Shoureshi, T. Knirek, P. Schilke, Optimal tuning of adaptive hydraulic engine mounts, SAE Paper 891160, 1989.
[15] B.H. Wilson, C. Erin, A. Messac, Optimal design of a vibration isolation mount using physical programming, Transactions of American Society of Mechanical Engineers, Journal of Dynamic Systems, Measurement, and Control 121 (1999) 171–178.
[16] H. Ashrafiuon, Design optimization of aircraft engine-mount systems, Transactions of American Society of Mechanical Engineers, Journal of Vibration and Acoustics 115 (1993) 463–467.
[17] Y. Yu, S.M. Peelamedu, N.G. Naganathan, R.V. Dukkipati, Automotive vehicle engine mounting systems: a survey, Transactions of American Society of Mechanical Engineers, Journal of Dynamic Systems Measurement and Control 123 (2001) 186–194.
[18] D. Hayashi, T. Satoh, T. Okita, Distributed optimization by using artificial life, Transactions of the Institute of Electrical Engineers of Japan 116-C (5) 1996.
[19] B.S. Yang, Y.H. Lee, Artificial life algorithm for function optimization, American Society of Mechanical Engineers Design Automation Conference, DAC-14524, 2000.

[20] B.S. Yang, Y.H. Lee, B.K. Choi, H.J. Kim, Optimum design of short journal bearing by artificial life algorithm, Tribology International 34 (2001) 427–435.
[21] B.S. Yang, J.D. Song, Enhanced artificial life algorithm for fast and accurate optimization search, Proceedings of the Asia-Pacific Vibration Conference, 2001, pp. 732–736.
[22] Optimization Toolbox for use with MATLAB, Version 2.i (Release 12), The Mathworks, Natick, MA, 2000.
[23] L.R. Miller, M. Ahmadian, Active mounts - a discussion of future technological trends, Proceedings of the Internoise 92 Conference, Toronto, Canada, 1992, pp. 421–426.
[24] P.J. Jones, Volume Compensated Fluid Mount, US Patent 4811919, Lord Corporation, Erie, PA, 1987.
[25] D.C. Karnopp, D.L. Margolis, R. Rosenberg, System Dynamics: A Unified Approach, 2nd Edition, Wiley, New York, 1990.
[26] N. Hu, Tabu search methods with random moves for globally optimal design, International Journal for Numerical Methods in Engineering 35 (1992) 1055–1070.